JACS
JOURNAL OF THE AMERICAN CHEMICAL SOCIETY
Article
pubs.acs.org/JACS

Coverage- and Temperature-Controlled Isomerization of an Imine Derivative on Au(111)

Cornelius Gahl,*[,†] Daniel Brete,[†,‡] Felix Leyssner,[†] Matthias Koch,[†,§] Erik R. McNellis,[∥] Johannes Mielke,[§] Robert Carley,[†,‡] Leonhard Grill,[§] Karsten Reuter,[⊥] Petra Tegeder,[†] and Martin Weinelt*[,†]

[†]Fachbereich Physik, Freie Universität Berlin, Arnimallee 14, 14195 Berlin, Germany
[‡]Max-Born-Institut, Max-Born-Str. 2A, 12489 Berlin, Germany
[§]Fritz-Haber-Institut der Max-Planck-Gesellschaft, Faradayweg 4-6, 14195 Berlin, Germany
[∥]Department of Molecular Spectroscopy, Max Planck Institute for Polymer Research, Ackermannweg 10, 55128 Mainz, Germany
[⊥]Lehrstuhl für Theoretische Chemie, Technische Universität München, Lichtenbergstr. 4, 85747 Garching, Germany

ABSTRACT: The isomerization behavior of photochromic molecular switches is strongly influenced by adsorption on metal surfaces. For (*E*)-3,5-di-*tert*-butyl-*N*-(3,5-di-*tert*-butyl-benzylidene)aniline (abbreviated as TBI for tetra-*tert*-butyl imine), it is found that a layer adsorbed on Au(111) can undergo an isomerization from the *trans* to the *cis* and back to the *trans* configuration when continuously increasing the sample temperature and accordingly decreasing the sample coverage. The conformation and adsorption geometry of TBI are determined from near-edge X-ray absorption fine structure measurements in agreement with density functional theory calculations taking into account the van der Waals interaction between adsorbate and metal surface. The coverage- and temperature-controlled conformational transitions are reversible and are driven by the higher packing density of the less stable *cis*-isomer in combination with the low thermal activation barrier of the *trans*- to *cis*-isomerization typical for imine derivatives. This unexpected scenario is corroborated by thermal desorption and vibrational spectroscopy as well as scanning tunneling microscopy.

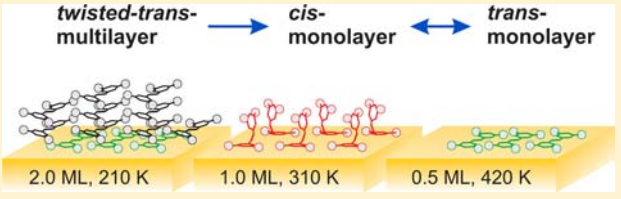

INTRODUCTION

Analysis and control of mechanical and electronic properties on the molecular scale are key challenges in nanoscience and nanotechnology. Here molecular switches offer unique building blocks to structure and tailor functional surfaces, with possible applications ranging from actuators[1−3] to organic transistors[4] and data processing.[5,6] While there exists a plethora of molecules that are bistable and reversibly switchable in solution, or when aggregated in multilayers and molecular crystals,[7] in contact with a surface many molecular switches become inoperative. At the surface the adsorbate's ground state is stabilized by bond formation and/or van der Waals interaction, and charge or energy transfer between adsorbate and substrate can lead to effective quenching of (photo)excited molecular states.[8−10] The isomerization properties of the molecular switch thus strongly depend on the surface orientation[11] and the local atomic structure underneath each individual molecule.[12] Besides these vertical adsorbate/substrate interactions the adsorption strength and geometry are often influenced by intermolecular interactions which may alter the adsorption geometry.[13,14] Such lateral interactions support self-organization and self-assembly of organic molecules[15−17] and are essential for the growth of functional molecular structures and networks.[18−21] In such self-assembled layers, intermolecular coupling and steric constraints may either suppress or promote conformational changes[12,22] and even lead to cooperative switching of the molecular ensemble as a whole.[23,24]

There are a number of examples where the coupling to the substrate and substrate excitations leads to new, functional properties. Ground-state conformations of adsorbed molecules have been found to differ from solution,[25−27] but these changes were unfortunately unalterable. A particular adsorbate system, where photoisomerization from the *trans*- to *cis*-conformation and thermal back reaction have been observed is 3,3′,5,5′-tetra-*tert*-butyl-azobenzene (TBA) adsorbed on Au(111).[28−33] The structural formula of TBA is shown in Figure 1. The *tert*-butyl groups are attached in *meta* position with the intention to decouple the frontier orbitals, responsible for the photoisomerization in the liquid phase,[34−36] from the substrate. In fact for TBA adsorbed on Au(111), a photostationary state with up to 70% *cis*-conformers has been achieved.[33,37] In contrast to photoswitching in solution, the *trans*−*cis* photoisomerization of TBA on Au(111) is not attributed to an intramolecular $\pi \rightarrow \pi^*$ transition but is most likely driven by a hole transfer from the gold d-bands to the highest occupied molecular orbital (HOMO) of the adsorbed TBA molecule.[31] Annealing of the Au(111) surface initiates the *cis*−*trans* back reaction, for which a

Received: September 20, 2012
Published: January 31, 2013

   dx.doi.org/10.1021/ja309330e | *J. Am. Chem. Soc.* 2013, 135, 4273−4281

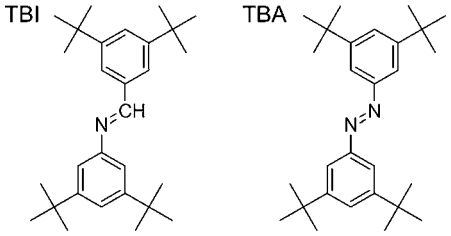

Figure 1. Structural formulas of (*E*)-3,5-di-*tert*-butyl-*N*-(3,5-di-*tert*-butylbenzylidene)aniline (TBI) and 3,3′,5,5′-tetra-*tert*-butyl-azobenzene (TBA). The *tert*-butyl groups are attached with the intention to decouple the molecules from the surface.

lower barrier is found compared to the reaction in solution.[32] While this demonstrates the importance of the gold substrate, (photo)isomerization of TBA is already suppressed on the related coinage metal surfaces Au(100),[11] Ag(111),[38] and Cu(111).[11] Obviously there exists a delicate interplay between the geometrical and electronic structure of the adsorbate/substrate complex and the concomitant adsorption energies, which rules the activity of the TBA photoswitch.[39,40]

An alternative route to modify the coupling and energetics of the molecular switch is to replace the diazo bridge −N═N− by a central imine group −HC═N−. For free *N*-benzylideneaniline and derivatives, calculated total energies of *cis*- and *trans*-isomers differ only by 0.2−0.3 eV and *cis*−*trans* activation barriers are on the order of 0.6 eV.[41] This leads to an increase of the thermal isomerization rates as confirmed by nuclear magnetic resonance experiments in solution.[41] Compared to azobenzene derivatives with a *cis*−*trans* thermal activation barrier of ∼1.0 eV the imine-bond facilitates thermal isomerization of the adsorbed molecules. In fact a recent study of the TBA analog, (*E*)-3,5-di-*tert*-butyl-*N*-(3,5-di-*tert*-butylbenzylidene)aniline (abbreviated as TBI for tetra-*tert*-butyl imine, see Figure 1) reveals that for low coverages on Au(111) individual molecules irreversibly adopt the *cis*-configuration upon annealing.[27]

In the present article we show that a layer of TBI molecules adsorbed on Au(111) can be almost completely converted upon heating and desorption from the *trans* to the *cis* and back to the *trans* configuration. Near-edge X-ray absorption fine-structure (NEXAFS) spectroscopy, high-resolution electron energy loss spectroscopy (HREELS), and scanning tunneling microscopy (STM) in combination with density functional theory (DFT) and thermal desorption spectroscopy (TDS) are used to determine the adsorption geometry and orientation of the aniline and benzylidene moiety of the different adsorbed isomers and their relative abundances within closed monolayers. While all layers are densely packed, the *cis*-geometry accommodates about 1.5 times more molecules per surface area than the *trans*-geometry. Since the *cis*-monolayer has a significantly higher density of adsorbed molecules than the *trans*-monolayer, the molecular conformation is not solely determined by the energy of the individual adsorbed molecule but is a consequence of the adsorption energy of the whole layer. At elevated temperature, TBI molecules can toggle between the two conformers, and the gain in total adsorption energy stabilizes the individually less favorable *cis*-isomer at high coverage. This interplay of low isomerization barrier and total adsorption energy leads to switching of nearly all molecules from *trans* to *cis* and back to *trans* configuration when varying the coverage upon annealing.

EXPERIMENTAL DETAILS

NEXAFS, HREELS, and STM experiments were carried out in three different UHV systems (base pressures $\leq 10^{-10}$ mbar), which all allow control of the sample temperature from 100 to 1000 K. The (111) surface of a gold single crystal was prepared by repeated cycles of Ar^+ sputtering (1 kV) and annealing to 800−900 K until low-energy electron diffraction (LEED) and/or STM showed clearly the herringbone reconstruction, and no carbon or sulfur contaminants were observed in XPS.

Molecular layers of TBI[41] were prepared by vapor deposition from effusion cells held at 370 K.[27] Coverage and layer structure of multilayers were controlled by dosing for a specific time at a sample temperature of 210 K. Monolayers can be prepared by adsorption of a multilayer of TBI and subsequent annealing to the specific temperature to desorb the excess molecules. Alternatively TBI can be dosed directly at an elevated sample temperature at which the desired layer structure forms until saturation coverage is reached. The latter preparation leads to the same overall structures and was favored for the NEXAFS measurements. TDS or STM is used to confirm the coverage of the investigated TBI layers. TDS was performed by heating the sample with a constant rate of 1 K/s. Desorbing molecules are detected by a quadrupol mass spectrometer set to the characteristic TBI fragments at m/e = 57 and 197 amu, corresponding to *tert*-butyl and di-*tert*-butyl-aniline moieties, respectively. The parent ion exceeds the mass range of m/e = 200 of our spectrometer.

The NEXAFS experiments were performed at the undulator beamline UE52-SGM of the synchrotron facility BESSY II (Helmholtz Zentrum, Berlin). Here the nitrogen KVV Auger yield was detected in an energy window of 5.0 eV centered at 377.0 eV. To determine the molecular orientation of *trans*- and *cis*-isomers, the sample was rotated around the X-ray beam axis. Thereby we record spectra with s- or p-polarized light and for a polarization direction corresponding to the magic angle of 54.7° with respect to the surface normal. To minimize beam damage, a fast shutter blocks the beam while stepwise scanning the monochromator and undulator. In parallel the photon flux is determined by a photodiode mounted on the shutter. All spectra are normalized to the photon flux and aligned at the N1s edge-jump. A detailed description of the HREELS and STM experiments has been given elsewhere.[27] NEXAFS and HREEL spectra were recorded at a sample temperature of 100 K, STM measurements were performed at 5 K.

THEORETICAL DETAILS

The DFT calculations were carried out with a locally modified version of the CASTEP code,[42] using the semilocal PBE exchange−correlation functional[43] together with the Tkatchenko−Scheffler dispersion correction scheme.[44] The computational details with respect to supercell geometry and numerical parameters are exactly the same as described in detail in our preceding work on azobenzene/TBA adsorption,[39,45,46] and we observed comparable convergence behavior as in these related systems. In order to further validate the semilocal PBE functional employed in the adsorption calculations, all gas-phase calculations reported below were additionally performed with the hybrid B3LYP functional[47] and a def2TZVPP basis set[48] in NWChem.[49] This did not yield any significant differences, neither with respect to the geometric nor the energetic PBE data reported below.

RESULTS

Thermal Desorption Spectroscopy. TDS is a primary method not only to determine the surface coverage of an adsorbate but also to gain insight into thermal and/or coverage driven structural transitions. Figure 2 shows the TD spectrum of TBI on Au(111) dosed at a sample temperature of 210 K. The molecules adsorbed in the second and higher layers desorb in the temperature range of 280−330 K, showing a zero-order

dx.doi.org/10.1021/ja309330e | J. Am. Chem. Soc. 2013, 135, 4273−4281

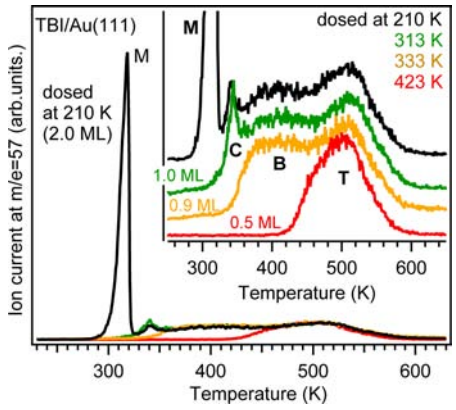

Figure 2. TDS of TBI on Au(111). Molecules in the multilayer (M) not in direct contact to the gold substrate desorb at $T < 310$ K. The three desorption peaks (see inset) are attributed to distinct monolayer structures C, B, and T with molecules in *cis*- and/or *trans*-configuration. The coverage of layer C is defined as $\Theta = 1.0$ ML.

desorption peak typical for multilayers. Molecules of the first monolayer interact directly with the metal substrate and are more strongly bound. They desorb over a very broad temperature interval of 320−600 K. This range is shown on an enlarged scale in the inset of Figure 2. The TD spectrum of the monolayer divides into three substructures, indicating that the monolayer of

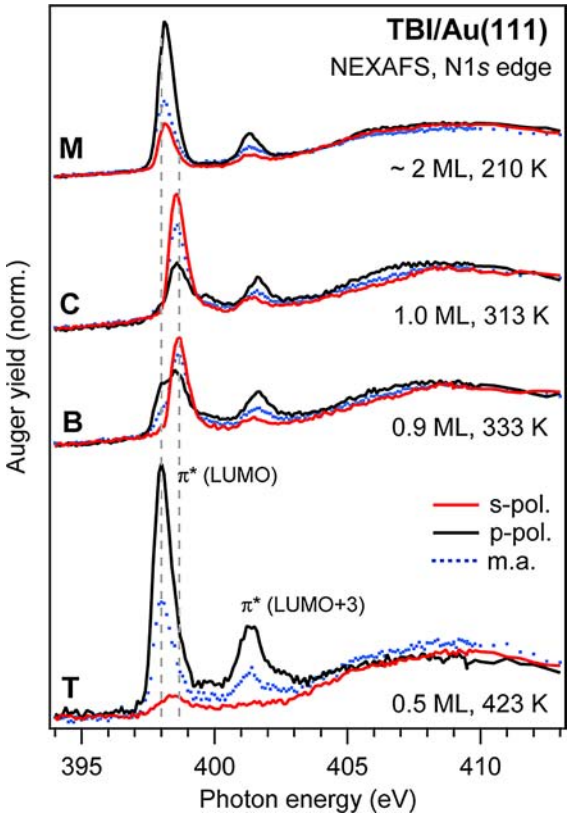

Figure 3. NEXAFS spectra recorded at the N1s-edge for TBI coverages of 2.0, 1.0, 0.9, and 0.5 ML, respectively. Note the different contrast of the distinct TBI layers for s- and p-polarization of the incident X-ray beam (red and black solid lines). Spectra recorded at the magic angle (m.a., 54.7°) between the X-ray polarization and the surface normal are shown as blue dots. All spectra have been normalized at photon energies above 423 eV to get the same N1s edge-jump intensity.

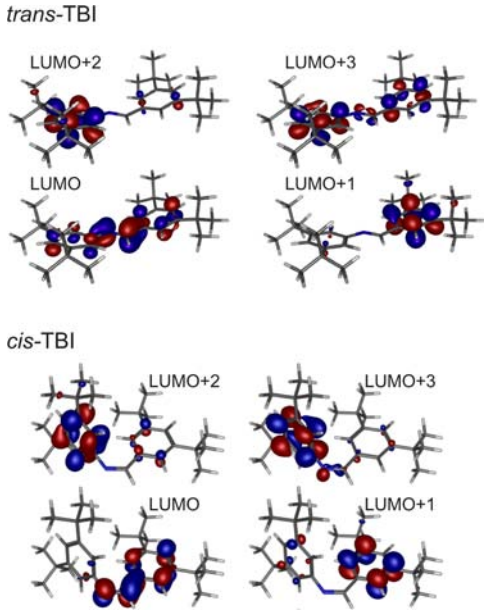

Figure 4. Contour plots of the four lowest unoccupied molecular orbitals of TBI in the planar *trans*- and the *cis*-configurations. Only the LUMO and LUMO+3 have significant electron density at the nitrogen atom.

TBI on Au(111) runs through three different layer structures C, B, and T during the heating process. The sharp peak at the onset of the monolayer desorption (here at 320 K) is frequently observed for adsorbate layers and is generally attributed to a compressed structure where molecules are shifted toward a less favorable adsorption site in order to place more molecules in direct contact to the substrate.[13,50]

As we will demonstrate below, the layers C, B, and T contain distinct fractions of *trans*- and *cis*-TBI molecules. Layers with the same characteristic adsorbate geometries can be directly prepared by dosing TBI at elevated sample temperatures until equilibrium coverage (Θ) is reached. The TD spectra of such layers prepared at 313, 333, and 423 K are shown in the inset of Figure 2. To specify the TBI coverage, we define the highest coverage corresponding to spectrum C as $\Theta = 1.0$ monolayer (ML) and determine the coverage of layers M (2.0 ML), B (0.9 ML), and T (0.5 ML) relative to this reference value by comparing the TDS peak integrals.

NEXAFS Spectroscopy. The configuration of the molecules and the orientation of the different molecular subunits as a function of coverage have been determined by NEXAFS spectroscopy.[51] Figure 3 displays absorption spectra recorded at the N1s-edge for coverages corresponding to the four TD spectra in Figure 2. The NEXAFS spectra were recorded with s- and p-polarized X-rays (red and black solid lines) and at the magic angle (m.a.; blue dots). In the latter measurement geometry the peak intensities become independent of the orientation of the transition dipole moments.[51]

To facilitate the structural assignment, the calculated contour plots of the four lowest unoccupied molecular orbitals (LUMOs) of TBI are shown in Figure 4 for the planar *trans*- and the *cis*-configuration. We immediately notice that independent of the conformer, only the LUMO and LUMO+3 have significant electron density at the nitrogen atom. Given the localized nature of the core−hole transition,[51] the corresponding N1s to π^* resonances must dominate the NEXAFS spectra of TBI at the nitrogen edge. From their relative intensities $I_{s,p}$ measured for the

dx.doi.org/10.1021/ja309330e | J. Am. Chem. Soc. 2013, 135, 4273−4281

Table 1. Structural Parameters of the Three Calculated TBI Configurations Optimized at PBE+TS Level of Theory (cf. Figure 7)[a]

	z_N (Å)	z_C(Å)	d_{CN} (Å)	CCNC (°)	α_C (°) theo.	α_C (°) exp.	α_N (°) theo.	α_N (°) exp.
t-trans	3.29	3.98	1.30	−170	32.5	(36 ± 3)	10.3	(34 ± 5)
trans	3.23	3.17	1.30	−169	11.5	15 ± 3	10.8	10 ± 3
cis	2.32	2.87	1.30	−3	82.0	71 ± 3	26.6	37 ± 5

[a]The bond length of the −HC═N− bridge is d_{CN}. The distance of the carbon and nitrogen atoms to the surface is z_N and z_C, respectively. CCNC describes the dihedral angle. The out-of-horizontal phenyl plane bend angles α_C and α_N are compared with the values derived from the NEXAFS experiment. The experimental values for the twisted *t-trans* configuration are extracted from the TBI multilayer data. The experimental values listed for the *trans*-configuration reflect the average orientation of the π-system ($\alpha_C \simeq \alpha_N$).

different polarizations (s and p) the angle α between the 1s to π^* transition dipole moment and the surface normal (cf. Figure 7) can be calculated:[52]

$$I_{s,p}/I_0 = P[\sin^2(\alpha)[1 - 3\cos^2(\beta)\cos^2(\theta)] + 2\cos^2(\beta)\cos^2(\theta)] + (1 - P)[\sin^2(\alpha)[1 - 3\sin^2(\beta)\cos^2(\theta)] + 2\sin^2(\beta)\cos^2(\theta)] \quad (1)$$

Here θ denotes the angle of incidence of the X-rays and β the rotation angle of the sample around the beam axis (β = 0° corresponds to p-polarization). The proportionality factor I_0 does not contain any angular dependence. The degree of linear polarization of the synchrotron radiation P is expected to be 96 ± 2%.[53] As seen from Figure 4, in the planar *trans*-configuration both LUMO and LUMO+3 resonances reflect the average tilt angle α of the conjugated π-system. In contrast in the *cis*-configuration the symmetry of the LUMO is determined by the orientation of the phenyl ring of the benzylidene moiety, while that of LUMO+3 reflects the orientation of the aniline moiety on the nitrogen side of the imine group. The transition dipole moments of N1s to LUMO and N1s to LUMO+3 are oriented perpendicular to the ring planes of the benzylidene and aniline moiety, respectively. Thus the characteristic NEXAFS spectra at the N1s-edge enable us to independently determine the out-of-surface-plane tilt angles α_C and α_N of the two phenyl rings in the *cis*-configuration.

We start our analysis with layer T at the lowest TBI coverage prepared by dosing the molecules at a sample temperature of 423 K. The corresponding N1s NEXAFS spectra at the bottom of Figure 3 are dominated by the main line at 398.0 eV, which corresponds to the resonant transition from the N1s core level of the imine bridge to the π^* LUMO. The second intense peak at 401.4 eV is assigned to the π^* LUMO+3 resonance. The additional weak structures at 399.7 and 402.3 eV are attributed to the LUMO+1,2 and LUMO+4,5 transitions. In the photon energy range of the continuum resonances above 405 eV, the spectra are rather featureless and exhibit negligible polarization dependence. In contrast, the transitions to LUMO and LUMO +3 show up as strong absorption peaks only for p-polarized X-rays, i.e., for an orientation of the electric field vector perpendicular to the surface. The intensity ratio of I_p/I_s = 15:1 of the N1s to π^* LUMO transition corresponds to an orientation of the transition dipole moment nearly normal to the surface. From Eq 1 we obtain an angle of α = 15 ± 3° between the imine group and the surface plane (see also Table 1). The polarization dependence of the N1s to π^* LUMO+3 resonance results in a comparable tilt angle of α = 10 ± 5°. In other words the imine group is aligned almost parallel to the surface plane, and accordingly the π-system of the adsorbed molecule remains conjugated (cf. Figure 4). We therefore conclude that for the low coverage of 0.5 ML the TBI molecules adopt the planar *trans*-configuration. This differs from the twisted *trans*-configuration (*t-trans*), which is the molecular ground state in the gas phase.[54]

For the densely packed monolayer C the N1s NEXAFS spectra look distinctly different. The peak at 398.0 eV photon energy is virtually missing. Instead the π^* LUMO resonance appears at $h\nu$ = 398.6 eV and, moreover, exhibits a reversed polarization dependence compared to layer T. The intensity ratio I_p/I_s = 1:2.3 (±0.3) corresponds to a transition dipole moment tilted by α_C = 71 ± 3° with respect to the surface normal. Likewise the transition from N1s to π^* LUMO+3 is shifted by 0.29 eV toward higher photon energies in the monolayer, but its polarization dependence changes only moderately when compared to layer T. The weaker contrast of the LUMO+3 resonances yields a bend angle of the aniline moiety of α_N = 37 ± 5° out of the surface plane. From the energetic shift of the π^* resonances alone, we must conclude that layer C and T contain different TBI species. From the different tilt angles α_C and α_N and the comparison with TBA/Au(111)[39] it stands to reason that the compressed monolayer *C* of TBI on Au(111) comprises the *cis*-isomers. The phenyl ring directly attached to the nitrogen, i.e., the aniline moiety, remains predominantly parallel to the metal surface. This geometry enables a stronger interaction of the nitrogen atom with the gold substrate. The opposite phenyl ring, i.e., the benzylidene moiety, is significantly rotated out of the surface plane (cf. Figure 7).

The NEXAFS spectra of adsorbate layer B, with a saturation coverage of Θ = 0.9 ML obtained by dosing TBI at 333 K, contain spectral contributions of both structures T and C. This means that the layer is made up from both *trans*- and *cis*-TBI species rather than consisting of a third adsorption complex. We can deduce the relative densities ρ_{trans} and ρ_{cis} of the two TBI species, supposing that the surface is still completely covered with TBI. The latter assumption will be substantiated by the STM measurements reported below.

$$\Theta_{trans}/\rho_{trans} + \Theta_{cis}/\rho_{cis} = \Theta^1_{trans}/\rho_{trans} = \Theta^1_{cis}/\rho_{cis} \quad (2)$$

$$\Theta = \Theta_{trans} + \Theta_{cis} \quad (3)$$

$\Theta_{trans,cis}$ denotes the coverages of the different isomers in the mixed layer, whereas $\Theta^1_{trans,cis}$ stands for the coverages in the respective pure monolayers. Now the intensity of a NEXAFS peak in the mixed layer relative to that of the pure *cis*-monolayer is given by

$$R = \frac{I_C}{I^1_C} = \frac{\Theta_{cis}/(\Theta_{cis} + \Theta_{trans})}{\Theta^1_{cis}/\Theta^1_{cis}} = \frac{\Theta_{cis}}{\Theta} \quad (4)$$

Here we take into account that the NEXAFS spectra are normalized to the X-ray absorption intensity well above the

dx.doi.org/10.1021/ja309330e | J. Am. Chem. Soc. 2013, 135, 4273−4281

ionization threshold, which is in good approximation proportional to the total coverage. The relative layer densities can then be written as

$$\frac{\rho_{cis}}{\rho_{trans}} = \frac{(\Theta^1_{cis} - \Theta_{cis})R}{\Theta_{cis}(1-R)} = \frac{\Theta^1_{cis} - R\Theta}{\Theta(1-R)} \quad (5)$$

In the mixed layer B the intensities of the N1s to π^* LUMO absorption peaks at 398.6 and 398.0 eV are 83 ± 2% and 17 ± 4% of their intensity for the respective pure layers. Accordingly the *cis*-layer has a significantly higher density than the *trans*-layer, $\rho_{cis} = (1.65 \pm 0.10)\cdot\rho_{trans}$.

Finally we turn to the TBI multilayer prepared by dosing 2.0 ML at a sample temperature of 210 K. The NEXAFS spectrum M in Figure 3 is again modified compared with those of layers T and C. The N1s to π^* LUMO transition now centers at an intermediate energy of 398.15 eV and does not simply consist of a superposition of the low- and high-density monolayer spectra C and T. Also the polarization dependence is different. While it delivers a mean orientation of the transition dipole moment preferentially perpendicular to the surface, the remaining intensity measured for s-polarized light corresponds to a tilt angle α_C of 36 ± 3°. A comparable tilt angle of α_N = 34 ± 5° results for the aniline moiety from the π^* LUMO+3 resonance. It is centered at a photon energy of 401.4 eV, equal to the low-density *trans*-monolayer. The comparable tilt angles of both aromatic rings suggest that in the multilayer M the majority of TBI molecules adopt the *trans*-configuration. From TDS we know that the molecules in the second layer are more weakly bound than those in the first layer. We thus reason that dosing TBI at low temperatures leads to a *trans*-monolayer, which is covered by an adlayer with the molecular axis oriented parallel to the surface but with a twisted configuration similar to the free *t-trans*-TBI molecule.

HREELS Spectroscopy. The derived model for the coverage and temperature controlled TBI configuration is also confirmed by HREELS experiments performed in a similar temperature sequence. Figure 5 shows HREELS spectra taken after deposition of 2.0 ML TBI at a sample temperature of 210 K and the subsequent annealing steps to 317 and 440 K. To elucidate the adsorption geometry, angular-dependent measurements in specular and 9° off-specular scattering geometries have been performed. Most striking are the pronounced intensity drops in the out-of-plane torsion modes of the phenyl rings (τ(C−C)) at 230, 703, and 875 cm^{-1} in the off-specular spectrum,[55] indicating that their intensities in the specular spectrum mainly originate from dipole scattering. The strong dipole activity of the phenyl rings' torsion modes arises from a molecular orientation in which the modes possess a strong dipole moment change upon vibration perpendicular to the substrate. This points toward an overall planar *trans* adsorption geometry of TBI at a multilayer coverage.

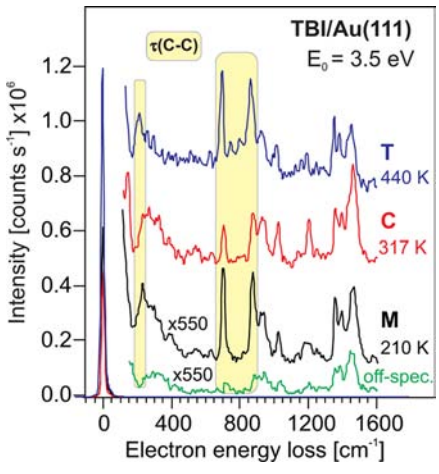

Figure 5. HREELS spectra of TBI on Au(111) recorded in specular and 9° off-specular scattering geometry with a primary electron energy of 3.5 eV. The resolution is ≤20 cm^{-1} (2.5 meV) for all measurements. The TBI multilayer was dosed at a sample temperature of 210 K. Subsequently the sample was annealed for 2 min at 317 or 440 K, using a heating rate of 1 K/s and cooled down to 100 K for the HREELS measurements. Highlighted are the phenyl rings' torsion modes (τ(C−C)), since they act as a sensitive probe of the isomerization state.

Annealing the sample to 317 K leads to a drastic intensity decrease of the phenyl rings' torsion modes, which we assign in line with the NEXAFS results to a conformational change to *cis*-isomers with one phenyl ring pointing upward. Finally, heating to 440 K leads to desorption of TBI as can be seen in Figure 2 and to a full recovery of the torsion modes. In agreement with the NEXAFS results, we conclude that desorbing *cis*-TBI from the surface results in a full monolayer in which the TBI adopts the *trans*-configuration.

STM. NEXAFS and HREELS both average over an ensemble of molecules. To verify the mixed *trans*/*cis* monolayer structure, STM investigations have been performed. Figure 6a,b shows STM measurements of TBI layers prepared by dosing a multilayer and subsequently annealing to 390 K for 10 min. As we know from previous studies on submonolayers of TBI[27] and TBA,[28] mainly the *tert*-butyl groups are imaged by STM. This is illustrated in Figure 6b where a magnified STM image is overlaid with structural formulas of the *trans*- and *cis*-species. In Figure 6 the *trans*-TBI molecule shows up as four dark-gray protrusions of comparable intensity, whereas the bright spots are characteristic for *cis*-TBI.[27] The latter is assigned to the *tert*-butyl legs of the tilted benzylidene moiety (cf. Figure 7).

The molecules, covering the entire surface, form well-ordered rows of *trans*-TBI interspersed by *cis*-TBI (Figure 6a). In the STM image the *cis*-isomers are preferentially found on the herringbone reconstruction, similar to the case of methoxy-TBA in a particular molecular arrangement[12] and probably due to the slight corrugation at these sites.[56] Figure 6b reveals that for each TBI molecule with *cis*-configuration, the azimuthal orientation of the neighboring *trans*-TBI molecules changes with respect to the row direction. This particular lateral stacking guarantees a dense packing of the molecules even in a mixed layer. On average 22 ± 2% of the molecules adopt the *cis*-configuration. Moreover, the *cis*-TBI molecules occupy less space on the surface. Careful analysis yields an area of 1.6 ± 0.1 nm^2 per *trans*-molecule, while *cis*-TBI requires a smaller area of only 1.1 ± 0.1 nm^2. Together with the dense packing of the TBI layer, this results in a ratio of *cis* vs *trans* layer densities of 1.5 ± 0.1 and a coverage of Θ = 0.74 ± 0.05 ML of the investigated layer. These findings substantiate our TDS and NEXAFS results.

THEORY

To understand the different, coverage-dependent adsorption geometries of the TBI molecule on Au(111) in more detail, we have performed first-principles DFT calculations. The starting point for the theory has been a systematic search for ground and metastable states of gas-phase TBI. In analogy to the related TBA molecule, this yields a *trans*-configuration with essentially planar imine bridge (i.e., CCNC angle = 177°) as the most stable state.

dx.doi.org/10.1021/ja309330e | J. Am. Chem. Soc. 2013, 135, 4273−4281

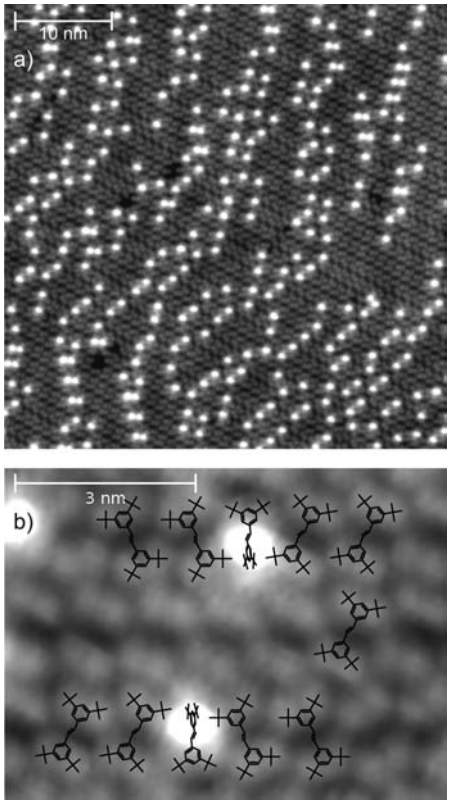

Figure 6. STM images of 0.74 ML TBI on Au(111) prepared by dosing a multilayer at T = 300 K and subsequent annealing at 390 K for 10 min. Measurement temperature is 5 K (V_{tip} = −0.55 V, I = 0.46 nA). (a) Overview, showing the dense packing of the molecules on the Au(111) surface. About 22% of TBI molecules adopt the *cis*-configuration. (b) STM image of three rows of *trans*-TBI molecules. In the top and bottom row a single *cis*-TBI molecule is intercalated and accommodated in a dense packing by an azimuthal realignment of the *trans*-TBI molecules. The structural formulas indicate *trans*- and *cis*-species.

In TBI, however, one phenyl moiety is twisted by 40° about the axis of the other, giving rise to an inherent molecular chirality. This leads to two *trans*-configurations, which are energetically degenerate in the gas phase and henceforth denoted as twisted *trans* (*t-trans*). The *cis*-configuration is metastable. Compared to TBA the energetic difference between *trans*- and *cis*-states is reduced by a factor of 2 (0.5 eV for TBA vs 0.24 eV for TBI).

The search for the preferred adsorption site was focused on the smaller *N*-benzylideneaniline molecule, assuming that the adsorption site is predominantly governed by the imine group−substrate interaction. Testing all high-symmetry sites offered by the Au(111) surface reveals the same preference for an atop 1:1 coordination of the nitrogen atom, as in case of both azobenzene and TBA.[39,45] Using this and the gas-phase geometries as the starting point for the surface calculations leads to the optimized adsorbed *t-trans* and *cis* geometries shown in Figure 7. In addition we also used a planar *trans*-configuration as the starting point for the geometry optimization, suspecting that such a configuration could be stabilized at the surface by the then enhanced van der Waals interaction with both phenyl moieties. This led to the planar *trans*-configuration also shown in Figure 7. Note that the planar *trans*- and the nonplanar *cis*-configurations are very similar to the TBA case.[11,39] The key structural parameters that characterize the three different adsorption geometries are summarized in Table 1.

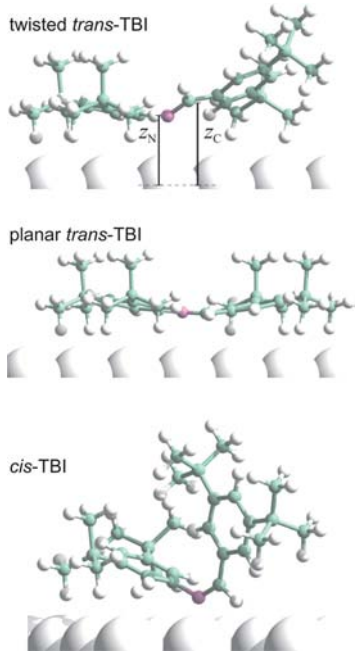

Figure 7. Illustration of the calculated adsorption geometries of TBI on Au(111) in the twisted *t-trans*-, planar *trans*-, and *cis*-configuration.

The frontier orbital structure of both the planar *trans*- and the *cis*-configuration is again essentially equivalent to the corresponding TBA cases. Figure 4 illustrates the four LUMOs of planar *trans*- and *cis*-TBI. We find no qualitative changes of these orbitals upon adsorption at Au(111) apart from some minor hybridization as detailed for azobenzene at coinage metals before.[45] This allows us to use the calculated gas-phase transition dipole moments to directly convert the measured NEXAFS data into geometric information concerning the orientation of the aniline and benzylidene moiety with respect to the surface normal.[22]

As suspected, the interaction with the Au(111) surface leads to a preferential stabilization of those configurations that maximize the van der Waals interaction with the underlying substrate. At the PBE+TS level of theory, we thus obtain a change in the energetic order with respect to the gas phase, with the planar *trans*-configuration resulting as most stable. As compiled in Figure 8 the *cis*-isomer is about 0.4 eV and the *t-trans*-isomer about 0.55 eV higher in energy. From the known shortcomings of the employed DFT dispersion-correction scheme with respect to

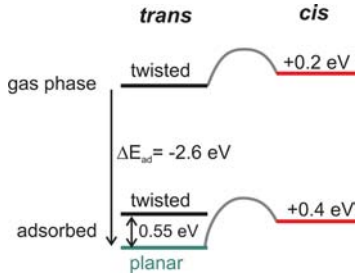

Figure 8. DFT-D energetics of TBI adsorbed on Au(111): Due to the interaction with the substrate the planar *trans*-conformation (green) becomes more stable than the *t-trans*-conformation (black), which represents the ground state in the gas phase. The energy gain by adsorption is thus bigger than the energy cost for isomerization to *cis* (red).

dx.doi.org/10.1021/ja309330e | *J. Am. Chem. Soc.* 2013, 135, 4273−4281

screening at metal surfaces we would expect this *trans*−*cis* energy gap $\Delta_{trans-cis}$ as well as the sizable adsorption energies of about 2 ∼eV of all three configurations, cf. Figure 8, to be substantially overestimated.[57] Even if this amounts to a factor of 2, however, there is no doubt that the absolute *trans* adsorption energy (2.63 eV) is considerably larger than the $\Delta_{trans-cis}$ energy gap (0.4 eV), which will be a key feature in the rationalization of the experimentally observed isomerization changes with coverage.

DISCUSSION

The NEXAFS, HREELS, and STM studies clearly demonstrate that TBI forms distinct monolayer structures which differ not only with respect to their mutual orientation but are also made up of different isomers.

For structure T we can clearly assign the molecular conformation as essentially planar *trans* with a twist angle smaller than 15°. In the case of the planar conformation the π^* orbitals extend over the whole conjugated moiety, and the NEXAFS spectra are very similar to those of *trans*-TBA on Au(111).[33] Similar adsorption behavior has been observed for TBA, dimethoxy-TBA, and tetra-*tert*-butyl-stilbene on Au(111) in HREEL spectroscopy.[58−60]

In contrast, for the TBI monolayer C with the highest coverage we find a monolayer structure consisting almost completely of a twisted molecular species. The orientation of the aniline and benzylidene moieties derived from NEXAFS, which averages over the ensemble of molecules, is in good agreement with the theoretical prediction for the individual *cis*-isomer (cf. Table 1). The out-of-surface-plane bend angles of the aniline and benzylidene moieties of 73° and 37° determined here agree very well with the assignments made.

For the TBI multilayer M the polarization dependence and the energetic position of the N1s to LUMO transition and the HREELS spectra are in accordance with a *trans*-conformation of the entire adsorbate layer. The reduced NEXAFS contrast and the energetic broadening suggest, however, that the molecules which are not in direct contact with the gold substrate adsorb in a twisted *t-trans*-conformation similar to the (calculated) gas-phase ground state. The molecules directly adsorbed on Au(111) most likely adopt the planar *trans*-geometry; based on NEXAFS and HREELS a *cis*-conformation of the molecules in the first layer can be ruled out, if adsorbed at ∼210 K.

So far we have discussed the molecular conformation only on the single molecule level. In the present case it is, however, especially interesting to understand the driving forces for the restructuring of the complete layer considering the ensemble of molecules. From STM studies at submonolayer coverages we know that TBI molecules aggregate at low temperatures in well-ordered islands in the planar *trans*-configuration.[27] Thus there is no long-range repulsive interaction between the molecules, and we can conclude that the saturation of the highest energy desorption peak T corresponds to a closed monolayer of *trans*-TBI. Up to this coverage we did not find significant amounts of *cis*-molecules in core-level spectroscopy even upon annealing up to 500 K. We estimate a detection limit of 3% of a *trans*-monolayer. Therefore we conclude that the planar *trans*-conformation is the stable isomer on a flat Au(111) terrace. We note that this result is not at variance with previous STM data which report on a *cis*-species upon annealing a submonolayer of TBI.[27] At the very low coverage studied in STM, the *cis*-TBI molecules are adsorbed at the herringbone ridges of the reconstructed Au(111) surface. Obviously there is a small amount of reactive sites below our NEXAFS detection limit which favor the *cis*-configuration of TBI. However, the vast majority of molecules in layer T are adsorbed in the *trans*-conformation. In addition the NEXAFS and HREELS data show that TBI also stays in a *trans*-configuration for multilayers adsorbed at temperatures below 250 K.

What processes lead to the *trans*−*cis* isomerization of the TBI molecules in the monolayer during thermal desorption of the multilayer? The answer can be given from the calculated adsorption energies for the two isomers. Even though the calculated adsorption energy is likely strongly overestimated,[39] even if corrected it will remain much larger than the energy difference between the adsorbed *trans*- and *cis*-isomers. This holds likewise for the activation barrier of the thermal *cis*- to *trans*-isomerization, which is only 0.6 eV for the molecule in solution[41] and is in analogy to TBA on Au(111) expected to be lower for the adsorbed molecule.[32,61] Therefore, if the *cis*-layer achieves a higher molecular density the gain in adsorption energy can overcompensate the energy penalty to switch the additional as well as the preadsorbed *trans*-TBI molecules. Hence a surplus of TBI molecules, either from a second layer or from the gas phase, drives the transformation of the *trans*- into the *cis*-layer. This isomerization explains also the abrupt change of the work function observed for the transition from multi- to monolayer.[62] As we have shown, the *cis*-monolayer has a 50% higher density than the *trans*-monolayer. Accordingly, the adsorption energy of one additional molecule has to exceed the energy to isomerize three TBI-molecules from *trans* into *cis*. Note that while the energy barrier of the *trans*−*cis* isomerization influences the rate of this switching process, the energy balance is only determined by the adsorption energies of *trans*- and *cis*-species. Our estimate does not yet include the energy contribution of intermolecular interactions. The latter probably favors neighboring *cis*-isomers, as they allow for parallel stacking of the π-systems of the upward tilted phenyl rings. Since the isomerization itself and an eventual reorganization of the layer are both activated processes, the transformation happens only at sufficiently high temperatures, for example, during a TDS heating ramp.

Taking into account the total adsorption energy for different coverages and molecular conformations, we deduce the model sketched in Figure 9. TBI molecules adsorb on a Au(111) surface at a temperature of 210 K in the *trans*-conformation independent of coverage. At low temperatures the molecules cannot overcome the activation barrier for an isomerization. Molecules in direct contact with the substrate will adopt a nearly planar form, while molecules in the second and higher layers maintain their *t-trans*-structure as in the gas phase. In the temperature range from 270 to 320 K the thermal energy is sufficient to drive two competing processes: the desorption of TBI molecules not directly attached to the gold substrate and a restructuring of the first adsorbate layer comprising *trans*−*cis* isomerization of TBI molecules and integration of additional molecules from the second into the first layer. When dosing TBI onto a Au(111) substrate at 313 K, adsorption from gas phase and desorption of weakly bound molecules reaches an equilibrium leaving a full, densely packed *cis*-monolayer of TBI on Au(111) after sufficiently long dosing times (Figure 9, right panel).

Toward higher temperatures molecules desorb out of the monolayer. The now uncovered surface area is filled by neighboring *cis*-molecules switching back to the *trans*-configuration. Upon annealing to 420 K or dosing at this temperature, TBI forms a well-ordered planar *trans*-monolayer. At coverages below a full *trans*-monolayer TBI molecules assemble in well-ordered islands.

dx.doi.org/10.1021/ja309330e | J. Am. Chem. Soc. 2013, 135, 4273−4281

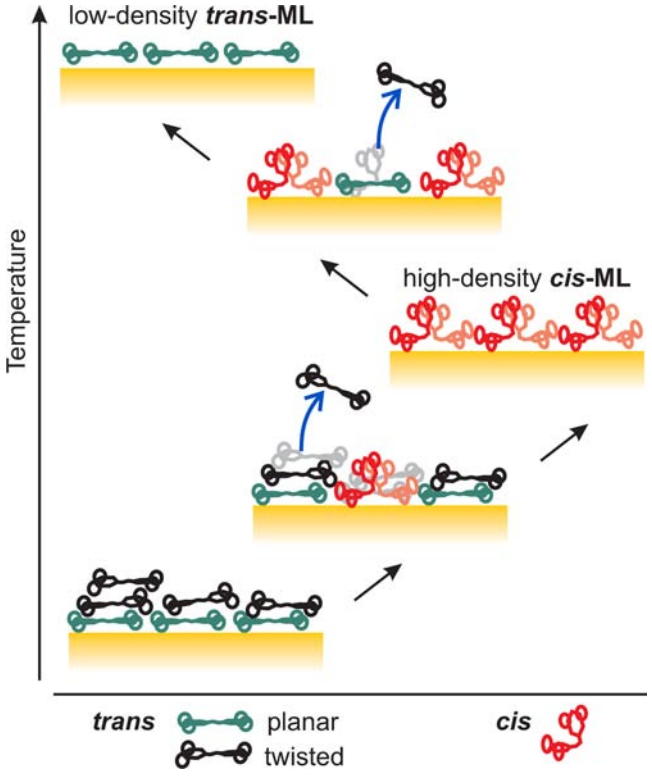

Figure 9. Schematics of the temperature and coverage driven isomerization of TBI on Au(111). Adsorbed at low temperatures the molecules on the surface switch from *trans* to *cis* and back to *trans* when continuously increasing the temperature due to the supply of activation energy and the change of coverage.

CONCLUSIONS

On the basis of TDS, NEXAFS, HREELS, and STM measurements in combination with DFT calculations, we have determined the molecular structure of the *trans*- and *cis*-isomer of TBI on the Au(111) surface. *Trans*-TBI adsorbs in a planar geometry with both phenyl rings oriented nearly parallel to the surface. In contrast the *cis*-isomer is characterized by a benzylidene moiety rotated by ∼70−80° out of the surface plane, while the aniline part remains moderately tilted ∼25−40°. Depending on their conformation, the molecules can form closed monolayers of different density on the Au(111) surface.

The planar *trans*-monolayer is thermally most stable. However, as the *cis*-isomer requires only two-thirds of the space of a *trans*-isomer when adsorbed on the surface, the total monolayer coverage can be increased by a factor of ∼1.5 incorporating more and more *cis*-TBI molecules. With increasing coverage the molecular layer gradually switches from a nearly complete *trans*- to a nearly complete *cis*-monolayer. The DFT calculations reveal that the main driving force for this isomerization reaction is the balance between total adsorption energy and the energy of the individual surface-bound isomer. We can conclude that for a constant TBI dose, i.e., partial pressure, the Au(111) surface will be covered either by *cis*- or *trans*-isomers or a mixture which is reversibly adjustable by the surface temperature. This effect is based on the interplay between the small thermal isomerization barrier of TBI, typical for the imine bond, and the smaller space required by the *cis*- as compared to the *trans*-isomer. As the layer transforms gradually with coverage and the cis-configuration is stabilized by coadsorption of neighboring molecules in a particular structural arrangement, the observed *trans*−*cis* isomerization of the TBI molecules is likely induced by molecular interactions.

AUTHOR INFORMATION

Corresponding Author

c.gahl@fu-berlin.de; weinelt@physik.fu-berlin.de

Notes

The authors declare no competing financial interest.

ACKNOWLEDGMENTS

We thank Ying Luo and Rainer Haag (Freie Universität Berlin) for providing us the imine derivative. Support by the Deutsche Forschungsgemeinschaft through Sfb 658, Elementary Processes in Molecular Switches at Surfaces, is gratefully acknowledged.

REFERENCES

(1) Liu, Z. F.; Hashimoto, K.; Fujishima, A. *Nature* **1990**, *347*, 658−660.
(2) Ferri, V.; Elbing, M.; Pace, G.; Dickey, M. D.; Zharnikov, M.; Samorì, P.; Mayor, M.; Rampi, M. A. *Angew. Chem., Int. Ed. Engl.* **2008**, *47*, 3407−3409.
(3) Kudernac, T.; Ruangsupapichat, N.; Parschau, M.; Macia, B.; Katsonis, N.; Harutyunyan, S. R.; Ernst, K.-H.; Feringa, B. L. *Nature* **2011**, *479*, 208−211.
(4) Crivillers, N.; Orgiu, E.; Reinders, F.; Mayor, M.; Samorì, P. *Adv. Mater.* **2011**, *23*, 1447−1452.
(5) Ikeda, T.; Tsutsumi, O. *Science* **1995**, *268*, 1873−1875.
(6) de Ruiter, G.; van der Boom, M. E. *Acc. Chem. Res.* **2011**, *44*, 563−573.
(7) *Molecular Switches*; Feringa, B. L., Ed.; Wiley-VCH: Weinheim, Germany, 2001.
(8) Lindstrom, C. D.; Zhu, X. Y. *Chem. Rev.* **2006**, *106*, 4281−4300.
(9) Kao, P.; Neppl, S.; Feulner, P.; Allara, D. L.; Zharnikov, M. *J. Phys. Chem. C* **2010**, *114*, 13766−13773.
(10) van der Molen, S. J.; Liljeroth, P. *J. Phys.: Condens. Matter* **2010**, *22*, 133001.
(11) Alemani, M.; Selvanathan, S.; Ample, F.; Peters, M. V.; Rieder, K.-H.; Moresco, F.; Joachim, C.; Hecht, S.; Grill, L. *J. Phys. Chem. C* **2008**, *112*, 10509−10514.
(12) Dri, C.; Peters, M. V.; Schwarz, J.; Hecht, S.; Grill, L. *Nat. Nanotechnol.* **2008**, *3*, 649−653.
(13) Huber, W.; Weinelt, M.; Zebisch, P.; Steinrück, H.-P. *Surf. Sci.* **1991**, *253*, 72−98.
(14) Kröger, I.; Stadtmüller, B.; Kleimann, C.; Rajput, P.; Kumpf, C. *Phys. Rev. B* **2011**, *83*, 195414.
(15) Schreiber, F. *Prog. Surf. Sci.* **2000**, *65*, 151−256.
(16) Love, J. C.; Estroff, L. A.; Kriebel, J. K.; Nuzzo, R. G.; Whitesides, G. M. *Chem. Rev.* **2005**, *105*, 1103−1169.
(17) Gooding, J. J.; Ciampi, S. *Chem. Soc. Rev.* **2011**, *40*, 2704−2718.
(18) Barth, J. V. *Annu. Rev. Phys. Chem.* **2007**, *58*, 375−407.
(19) Madueno, R.; Räisänen, M. T.; Silien, C.; Buck, M. *Nature* **2008**, *454*, 618−621.
(20) Bombis, C.; Weigelt, S.; Knudsen, M. M.; Nørgaard, M.; Busse, C.; Lægsgaard, E.; Besenbacher, F.; Gothelf, K. V.; Linderoth, T. R. *ACS Nano* **2010**, *4*, 297−311.
(21) Otero, R.; Gallego, J. M.; Vázquez de Parga, A. L.; Martín, N.; Miranda, R. *Adv. Mater.* **2011**, *23*, 5148−5176.
(22) Gahl, C.; Schmidt, R.; Brete, D.; McNellis, E.; Freyer, W.; Carley, R.; Reuter, K.; Weinelt, M. *J. Am. Chem. Soc.* **2010**, *132*, 1831−1838.
(23) Pace, G.; Ferri, V.; Grave, C.; Elbing, M.; von Hänisch, C.; Zharnikov, M.; Mayor, M.; Rampi, M. A.; Samorì, P. *Proc. Natl. Acad. Sci. U.S.A.* **2007**, *104*, 9937−9942.
(24) Crivillers, N.; et al. *Phys. Chem. Chem. Phys.* **2011**, *13*, 14302−14310.
(25) Piantek, M.; Miguel, J.; Krüger, A.; Navío, C.; Bernien, M.; Ball, D. K.; Herrmann, K.; Kuch, W. *J. Phys. Chem. C* **2009**, *113*, 20307−20315.

(26) Piantek, M.; Schulze, G.; Koch, M.; Franke, K. J.; Leyssner, F.; Krüger, A.; Navío, C.; Miguel, J.; Bernien, M.; Wolf, M.; Kuch, W.; Tegeder, P.; Pascual, J. I. *J. Am. Chem. Soc.* **2009**, *131*, 12729−12735.
(27) Mielke, J.; Leyssner, F.; Koch, M.; Meyer, S.; Luo, Y.; Selvanathan, S.; Haag, R.; Tegeder, P.; Grill, L. *ACS Nano* **2011**, *5*, 2090−2097.
(28) Alemani, M.; Peters, M. V.; Hecht, S.; Rieder, K.-H.; Moresco, F.; Grill, L. *J. Am. Chem. Soc.* **2006**, *128*, 14446−14447.
(29) Hagen, S.; Leyssner, F.; Nandi, D.; Wolf, M.; Tegeder, P. *Chem. Phys. Lett.* **2007**, *444*, 85−90.
(30) Comstock, M. J.; Levy, N.; Kirakosian, A.; Cho, J.; Lauterwasser, F.; Harvey, J. H.; Strubbe, D. A.; Fréchet, J. M. J.; Trauner, D.; Louie, S. G.; Crommie, M. F. *Phys. Rev. Lett.* **2007**, *99*, 038301.
(31) Hagen, S.; Kate, P.; Leyssner, F.; Nandi, D.; Wolf, M.; Tegeder, P. *J. Chem. Phys.* **2008**, *129*, 164102.
(32) Hagen, S.; Kate, P.; Peters, M. V.; Hecht, S.; Wolf, M.; Tegeder, P. *Appl. Phys. A: Mater. Sci. Process.* **2008**, *93*, 253−260.
(33) Schmidt, R.; Hagen, S.; Brete, D.; Carley, R.; Gahl, C.; Dokic, J.; Saalfrank, P.; Hecht, S.; Tegeder, P.; Weinelt, M. *Phys. Chem. Chem. Phys.* **2010**, *12*, 4488−4497.
(34) Nägele, T.; Hoche, R.; Zinth, W.; Wachtveitl, J. *Chem. Phys. Lett.* **1997**, *272*, 489−495.
(35) Ishikawa, T.; Noro, T.; Shoda, T. *J. Chem. Phys.* **2001**, *115*, 7503−7513.
(36) Cembran, A.; Bernardi, F.; Garavelli, M.; Gagliardi, L. *J. Am. Chem. Soc.* **2004**, *126*, 3234−3243.
(37) Hagen, S. Isomerization behavior of photochromic molecules in direct contact with noble metal surfaces, Ph.D. thesis, Freie Universität Berlin, Berlin, Germany, 2009.
(38) Tegeder, P.; Hagen, S.; Leyssner, F.; Peters, M. V.; Hecht, S.; Klamroth, T.; Saalfrank, P.; Wolf, M. *Appl. Phys. A: Mater. Sci. Process.* **2007**, *88*, 465−472.
(39) McNellis, E. R.; Bronner, C.; Meyer, J.; Weinelt, M.; Tegeder, P.; Reuter, K. *Phys. Chem. Chem. Phys.* **2010**, *12*, 6404−6412.
(40) McNellis, E. R.; Mercurio, G.; Hagen, S.; Leyssner, F.; Meyer, J.; Soubatch, S.; Wolf, M.; Reuter, K.; Tegeder, P.; Tautz, F. S. *Chem. Phys. Lett.* **2010**, *106*, 247−249.
(41) Luo, Y.; Utecht, M.; Dokić, J.; Korchak, S.; Vieth, H.-M.; Haag, R.; Saalfrank, P. *ChemPhysChem* **2011**, *12*, 2311−2321.
(42) Clark, S. J.; Segall, M. D.; Pickard, C. J.; Hasnip, P. J.; Probert, M. I. J.; Refson, K.; Payne, M. C. *Z. Kristallogr.* **2005**, *220*, 567.
(43) Perdew, J. P.; Burke, K.; Ernzerhof, M. *Phys. Rev. Lett.* **1996**, *77*, 3865−3868.
(44) Tkatchenko, A.; Scheffler, M. *Phys. Rev. Lett.* **2009**, *102*, 073005.
(45) McNellis, E.; Meyer, J.; Baghi, A. D.; Reuter, K. *Phys. Rev. B* **2009**, *80*, 035414.
(46) McNellis, E. R.; Meyer, J.; Reuter, K. *Phys. Rev. B* **2009**, *80*, 205414.
(47) Becke, A. D. *J. Chem. Phys.* **1993**, *98*, 5648−5652.
(48) Weigend, F.; Ahlrichs, R. *Phys. Chem. Chem. Phys.* **2005**, *7*, 3297−3305.
(49) Valiev, M.; Bylaska, E.; Govind, N.; Kowalski, K.; Straatsma, T.; van Dam, H.; Wang, D.; Nieplocha, J.; Apra, E.; Windus, T.; de Jong, W. *Comput. Phys. Commun.* **2010**, *181*, 1477−1489.
(50) Schlichting, H.; Menzel, D. *Surf. Sci.* **1992**, *272*, 27−33.
(51) Stöhr, J. *NEXAFS Spectroscopy*; Springer-Verlag: Berlin, Germany, 1996.
(52) Outka, D. A.; Stöhr, J.; Rabe, J. P.; Swalen, J. D. *J. Chem. Phys.* **1988**, *88*, 4076−4087.
(53) Jung, C.; Eggenstein, F.; Hartlaub, S.; Follath, R.; Schmidt, J. S.; Senf, F.; Weiss, M. R.; Zeschke, T.; Gudat, W. *Nucl. Instr. Meth. A* **2001**, *467*, 485−487.
(54) Bürgi, H.; Dunitz, J. *Helv. Chim. Acta* **1970**, *52*, 1747−1764.
(55) Meic, Z.; Basanovic, G. *Pure Appl. Chem.* **1989**, *61*, 2129−2138.
(56) Barth, J. V.; Brune, H.; Ertl, G.; Behm, R. J. *Phys. Rev. B* **1990**, *42*, 9307−9318.
(57) Mercurio, G.; McNellis, E. R.; Martin, I.; Hagen, S.; Leyssner, F.; Soubatch, S.; Meyer, J.; Wolf, M.; Tegeder, P.; Tautz, F. S.; Reuter, K. *Phys. Rev. Lett.* **2010**, *104*, 036102.
(58) Óvári, L.; Wolf, M.; Tegeder, P. *J. Phys. Chem. C* **2007**, *111*, 15370−15374.
(59) Óvári, L.; Schwarz, J.; Peters, M. V.; Hecht, S.; Wolf, M.; Tegeder, P. *Int. J. Mass Spectrom.* **2008**, *277*, 223−228.
(60) Leyssner, F.; Hagen, S.; Óvári, L.; Dokić, J.; Saalfrank, P.; Peters, M.; Hecht, S.; Klamroth, T.; Tegeder, P. *J. Phys. Chem. C* **2010**, 1231−1239.
(61) Maurer, R. J.; Reuter, K. *Angew. Chem., Int. Ed.* **2012**, *51*, 12009−12011.
(62) Hagen, S.; Luo, Y.; Haag, R.; Wolf, M.; Tegeder, P. *New J. Phys.* **2010**, *12*, 125022.